Photodissociation Dynamics of CHF_2Cl after Photoexcitation at the Lyman-α Wavelength (121.6 nm)

Richard A. Brownsword, Matthias Hillenkamp, Thomas Laurent, Rajesh K. Vatsa,† Hans-Robert Volpp,* and Jürgen Wolfrum

Physikalisch-Chemisches Institut der Universität Heidelberg, Im Neuenheimer Feld 253, D-69120 Heidelberg, Germany

Received: July 31, 1996[⊗]

The collision-free gas-phase photodissociation dynamics of CHF_2Cl (HCFC-22) were studied at room temperature using the laser photolysis/laser-induced fluorescence "pump/probe" technique. Lyman-α laser radiation ($\lambda = 121.6$ nm) was used both to photodissociate the parent molecule and to detect the nascent H atom products via ($2p^2P \leftarrow 1s^2S$) laser-induced fluorescence. An absolute H atom quantum yield of $\Phi_H = 0.77 \pm 0.13$ was determined by a calibration method in which H_2O photolysis at 121.6 nm was used as a reference source of well-defined H atom concentrations. The line shapes of the measured H atom Doppler profiles indicate a bimodal velocity distribution suggesting the presence of two different H atom formation pathways in the Lyman-α photodissociation of CHF_2Cl.

Introduction

As a result of the worldwide effort to design replacements for the chlorofluorocarbons (CFCs) which have been implicated in the ozone destruction in the stratosphere,[1] a variety of substitutes have been developed.[2] For many applications hydrochlorofluorocarbons (HCFCs) are being recognized as "environmentally friendly" replacements. HCFCs have at least one C−H bond and can therefore be oxidized by OH radicals in the troposphere, preventing them from entering the stratosphere. However, a big increase in the atmospheric concentration of for example CHF_2Cl (HCFC-22), which is currently used in industry as a replacement for CCl_2F_2 (CFC-12) and C_2F_5Cl (CFC-115), has been observed between the first Atmospheric Trace Molecule Spectroscopy (ATMOS) experiment flight in 1985 and the Atmospheric Laboratory for Applications and Science (ATLAS-3) mission in 1994.[3] According to model calculations, CHF_2Cl will soon become the dominant source of odd chlorine in the atmosphere above 40 km if the global emission rate remains unabated.[4] Thus, investigations of the ultraviolet (UV) and vacuum-ultraviolet (VUV) photochemistry and in particular measurements of photolysis product branching ratios for this compound are clearly needed.

The UV and VUV photodissociation dynamics of the HCFCs have rarely been studied,[5] and the latter in particular has yet to be characterized experimentally. UV absorption cross sections of $CHFCl_2$ (HCFC-21) and CHF_2Cl were measured by several groups.[6−8] Huber and co-workers[9] carried out detailed studies of the $CHFCl_2$ UV photodissociation ($\lambda_{photo} = 193$ nm) using photofragment translational spectroscopy and found that, at this wavelength, C−Cl bond fission is the primary photolytic process. Recently, CHF_2Cl photodissociation dynamics studies were carried out by Melchior et al. at the same UV wavelength.[10] In these studies a channel producing H atoms was observed besides $Cl(^2P_{3/2})$ and $Cl(^2P_{1/2})$ formation. Using time-of-flight mass spectrometry (TOF-MS) in combination with (2 + 1) resonance-enhanced multiphoton ionization (REMPI) product detection, they measured a $H/\{Cl(^2P_{3/2}) + Cl(^2P_{1/2})\}$ branching ratio of 0.19 ± 0.06. In the same studies an upper limit of 1% for the HCl elimination channel was reported. VUV absorption and photoelectron spectra (200−120 nm) of CHF_2Cl were reported by Doucet et al.[11] and Gilbert et al.[12] extended the absorption measurements down to 65 nm. However, no information about the photochemical reaction products was reported for that photolysis wavelength region. The aim of the work to be presented in this article is to provide experimental dynamical quantities such as a photolytic H atom yield and information about the energy partitioning in the VUV photolysis of CHF_2Cl. The Lyman-α wavelength was chosen owing to its very strong presence in the solar emission spectrum[1] and because of the possibility for simultaneous H atom product detection via ($2p^2P \leftarrow 1s^2S$) laser-induced fluorescence (LIF).

Experiment

The photodissociation studies were carried out in a flow apparatus (schematically depicted in Figure 1), which is similar to the one used in bimolecular reaction dynamics studies of the $O(^1D) + H_2/D_2/HD$[13a] and OH + CO[14] reactions. Room temperature CHF_2Cl (Messer Griesheim, 99.9%) was pumped through the reactor without further purification. The CHF_2Cl flow was controlled by a Tylan flowmeter. For the calibration measurement H_2O (deionized and double distilled) was passed through the reactor. The H_2O flow was regulated by a glass valve. Typical pressures during the photodissociation experiments were 60−90 mTorr as measured by an MKS Baratron.

VUV laser light—tunable around the H atom Lyman-α transition at 121.567 nm—was generated by resonant third-order sum-difference frequency conversion of pulsed-dye-laser radiation in a phase-matched Kr−Ar mixture[15] and used to photodissociate the CHF_2Cl molecule as well as to detect the photolytically produced H atom via ($2p^2P \leftarrow 1s^2S$) laser-induced fluorescence (LIF) within the same laser pulse. The duration of the laser pulse was about 15 ns (as indicated in Figure 1). The Kr mixing scheme via which the VUV radiation ($\omega_{VUV} = 2\omega_R - \omega_T$) was generated is included as an inset in Figure 1. The laser radiation of ω_R ($\lambda_R = 212.55$ nm) is resonant with the Kr 4p−5p ($^1/_2$,0) two-photon transition and was held fixed during the experiments, while ω_T was tuned from 844 to 846 nm to generate VUV radiation covering the H atom Lyman-α

† On sabbatical leave from Chemistry Division, Bhabha Atomic Research Centre, Bombay, India.

* To whom correspondence should be addressed.

[⊗] Abstract published in *Advance ACS Abstracts,* January 1, 1997.

S1089-5639(96)02330-4 CCC: $14.00

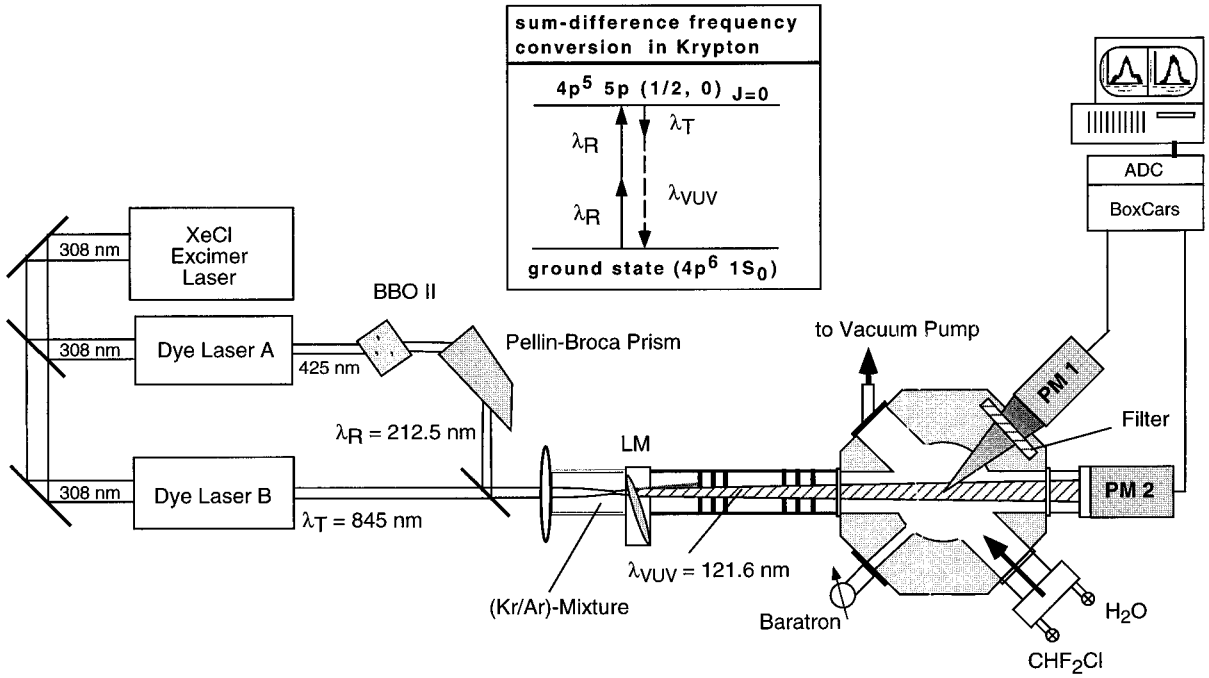

Figure 1. Experimental apparatus used for the CHF_2Cl VUV photolysis studies. The Kr four-wave mixing scheme for VUV generation is shown as an inset. (Details are explained in the text.)

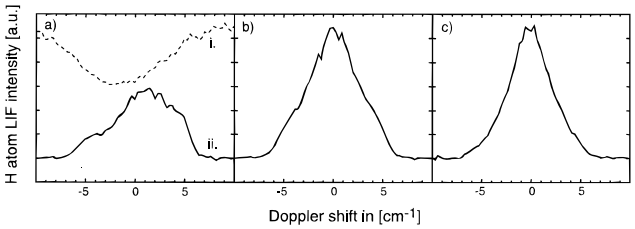

Figure 2. Doppler profiles of H atoms. (a) Curve i is the measured Lyman-α laser intensity change, and curve ii is the measured H atom LIF signal obtained in the CHF_2Cl (85 mTorr) photolysis. (b) The same H atom Doppler profile after normalization to the square of the Lyman-α laser intensity. (c) A normalized H atom Doppler profile obtained in the H_2O (65 mTorr) photolysis. The centers of the LIF spectra correspond to the Lyman-α transition for the H atom (82 259 cm^{-1}).

transition. The fundamental laser radiation was obtained from two dye lasers (Lambda Physik FL 2002), simultaneously pumped by a XeCl excimer laser (Lambda Physik EMG 210 MSC). In dye laser A Coumarin 120 was used to generate the 425.10 nm radiation which was subsequently frequency doubled in a BBO II crystal in order to obtain $\lambda_R = 212.55$ nm. $\lambda_T =$ 844−846 nm was obtained directly by operating dye laser B with Styryl 9 dye.

The generated Lyman-α light was carefully separated from the fundamental laser light by a lens monochromator (denoted as LM in Figure 1) followed by a light baffle system. The H atom LIF signal was measured through a band-pass filter (ARC, Model 122-VN-ID, $\lambda_{center} = 122$ nm, fwhm = 20 nm) by a solar blind photomultiplier (Hamamatsu Model R1259, denoted as PM 1 in Figure 1) positioned at right angles to the VUV laser beam. The VUV beam intensity was monitored after passing through the reaction cell with an additional solar blind photomultiplier of the same kind (PM 2 in Figure 1). In order to obtain a satisfactory signal-to-noise (S/N) ratio, each point of the H atom Doppler profiles (Figure 2) was averaged over 30 laser shots. The measurements were carried out at a laser repetition rate of 6 Hz. The LIF signals and the VUV beam intensity were recorded with a two-channel boxcar integrator system (SRS 250) and transferred to a microcomputer—via an analog-to-digital converter (SRS 235)—where the LIF signal was normalized point-by-point to the square of the VUV laser intensity. In Figure 2a the "raw" H atom LIF signal is shown (ii) together with the recorded Lyman-α laser intensity (i). Figure 2b shows the H Doppler profile which results from normalizing curve (ii) to the square of the Lyman-α laser intensity (i). In Figure 2c a H atom Doppler profile from the H_2O photolysis is shown which has been obtained using the same normalization procedure. Bearing in mind that sequential multiphoton absorption ($n > 2$) may distort the results, the ($n = 1 + 1$)-photon nature (one-photon dissociation of the parent molecule followed by one-photon H atom LIF detection) of the process was checked directly in separate experiments by varying the VUV laser intensity. Log−log plots of the measured H atom LIF signal versus the VUV laser intensity—as depicted in Figure 3—yielded slopes of $n = 2.1 \pm 0.2$ and $n = 1.9 \pm 0.1$ in the case of CHF_2Cl and H_2O photolysis, respectively. It is therefore concluded that secondary dissociation of photolysis products is negligible and need not be considered in the analysis of the results. Optical absorption cross sections of CHF_2Cl and H_2O at the Lyman-α wavelength were also measured in the course of the present experiments. The following values were obtained: $\sigma_{L_\alpha}(CHF_2Cl) = (1.8 \pm 0.2) \times 10^{-17}$ cm^2 and $\sigma_{L_\alpha}(H_2O) = (1.6 \pm 0.2) \times 10^{-17}$ cm^2.

Results

H Atom Quantum Yield. The absolute quantum yield Φ_H for photolytic H atom formation was obtained by calibrating the H atom signal $S_H(CHF_2Cl)$ measured in the CHF_2Cl photodissociation against the H atom signal $S_H(H_2O)$ from well-defined H atom number densities generated by photolyzing H_2O. The H_2O photodissociation has been extensively studied,[16] and recently the Lyman-α photodissociation dynamics was investigated in great detail.[17] In the present study, the absolute H atom quantum yield was determined using the following equation:

$$\Phi_H = \{S_H(CHF_2Cl)\ \Phi^*_H \sigma_{H_2O} p_{H_2O}\}/ \{S_H(H_2O)\ \sigma_{CHF_2Cl} p_{CHF_2Cl}\} \quad (1)$$

where σ_{H_2O} and σ_{CHF_2Cl} are the absorption cross sections of H_2O

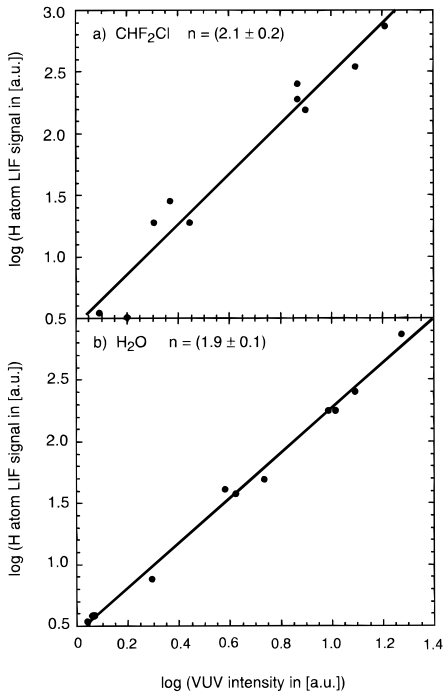

Figure 3. Dependence of the measured H atom LIF signal on the Lyman-α laser intensity: (a) for CHF_2Cl (62 mTorr) and (b) for H_2O (90 mTorr). *n* are the slopes of the linear log−log plots.

and CHF_2Cl at Lyman-α wavelength. Φ^*_H is the absolute H atom branching ratio in the Lyman-α photolysis of H_2O, which has been reported to be 1.02.[18] S_H is the integrated area under the measured H atom Doppler profiles, and p_{H_2O} and p_{CHF_2Cl} are the pressures of H_2O and CHF_2Cl, respectively.

In Figure 2, typical H atom Doppler profiles from the Lyman-α photodissociation of CHF_2Cl (b) and H_2O (c) are shown. In independent calibration runs, integrated areas under the fluorescence curve were determined for the H_2O and CHF_2Cl photodissociation under identical experimental conditions which gave—using eq 1—an average value of $\Phi_H = (0.77 \pm 0.13)$.

H Atom Translational Energy Release. From the H atom Doppler profile the first direct quantity of interest, the average kinetic energy (E_T) of the H atoms in the laboratory frame, was determined. Because the measured H atom Doppler profile reflects directly, via the linear Doppler shift $\nu - \nu_0 = \upsilon_z\nu_0/c$, the distribution of the velocity component υ_z of the absorbing H atoms along the propagation direction of the probe laser beam, the average translational energy is given (assuming a spatially isotropic velocity distribution) by $E_T = {}^3/_2 m_H\langle\upsilon_z^2\rangle$, where $\langle\upsilon_z^2\rangle$ represents the second moment of the laboratory velocity distribution of the H atoms. Evaluation of the measured profiles by a direct calculation of the second moment gave a value of $E_T = 140 \pm 2$ kJ/mol. Although this value is the one of practical atmospheric interest, because it determines the total amount of energy the photolytically produced atoms introduce, a more detailed analysis of the profiles was carried out in order to obtain more information about the underlying dissociation mechanism. The measured H atom Doppler profiles (all of them show a clear bimodal structure) were therefore fitted—following the suggestion of Matsumi and co-workers[19]—by a superposition of a wide non-Gaussian component which describes a speed distribution centred at a high velocity and a narrow Gaussian component which corresponds to a statistical Maxwell−Boltzmann-like velocity distribution. The results of such a numerical least-squares fit to a measured Doppler profile are shown in Figure 4a. The average width (fwhm) of the non-Gaussian contribution (represented in our case by a symmetric double sigmoidal function) was 10.7 ± 0.6 cm^{-1}, and that of the Gaussian was 4.5 ± 0.3 cm^{-1}. In Figure 4 the two translational energy distributions $P(E_T)$ are depicted (solid lines) which correspond to the non-Gaussian (Figure 4b) and the Gaussian component (Figure 4c), respectively. Evaluation of the two translational energy distributions yielded average values of $E_{T(non-G)} = 207 \pm 10$ kJ/mol and $E_{T(G)} = 74 \pm 15$ kJ/mol for the non-Gaussian and Gaussian components of the Doppler profile, respectively. The ratio of the areas of the two different Doppler profile contributions (non-Gaussian divided by Gaussian) was determined to be $\Gamma_{non-G}/\Gamma_G = 1.0 \pm 0.3$. The quoted uncertainties reflect one standard deviation of the values (Gaussian and non-Gaussian widths and areas, respectively) obtained in the evaluation of the complete set of measured profiles. The quality of each individual Doppler profile fit was much higher, as can be seen in Figure 4a, and in no case was a systematic trend in the residuals of the fit observed.

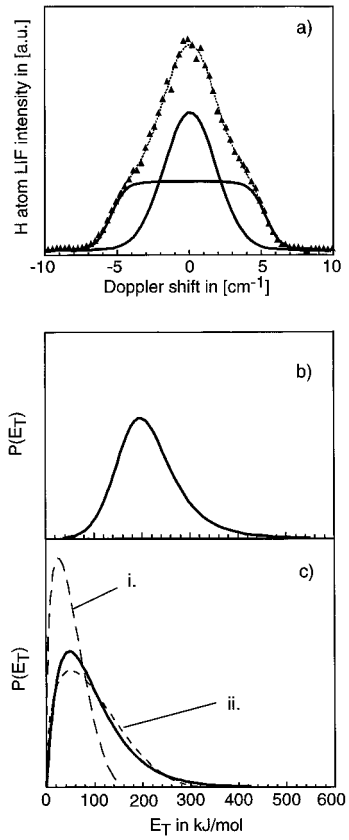

Figure 4. (a) Result of the fit of the composite function (as defined in the text) to the measured bimodal H atom Doppler profile (solid triangles). (b) H atom translational energy distribution $P(E_T)$ which corresponds to the nonstatistical (non-Gaussian) component of the measured profile. Solid line in (c) is the H atom translational energy distribution which belongs to the statistical (Gaussian) component of the measured profile. The two dashed lines are statistical "prior" distributions for the $CHF_2Cl \rightarrow CClF + F + H$ (i) and $CHF_2Cl \rightarrow CF_2 + Cl + H$ (ii) fragmentation pathway.

Discussion

An absolute H atom quantum yield of $\Phi_H = 0.77 \pm 0.13$ has been measured for the VUV photolysis of CHF_2Cl at the Lyman-α wavelength ($\lambda_{L_\alpha} \sim 121.6$ nm). At a photolysis wavelength of 193 nm (using an ArF excimer laser and the background subtraction method described in ref 13b), we were unable to detect H atoms, attributable to direct photolytic H atom formation at that wavelength. On the basis of the S/N ratio and the H atom LIF signals that we were able to observe from the 193 nm photodissociation of very low HCl concentrations ($p_{HCl} \approx 1-2$ mTorr), we could determine, however, an

upper limit of 0.1 for the direct photolytic H atom quantum yield at 193 nm. From the much more sensitive (2 + 1) REMPI-TOF-MS measurements of Melchior et al.[10] at the photolysis wavelength of 193 nm, a value of $\Phi_H = 0.16 \pm 0.05$ can be derived assuming that $\Phi_H + \Phi_{Cl/Cl^*} = 1$.

The above results clearly show the increasing importance of H atom formation with decreasing wavelength in the photodissociation of CHF_2Cl. This is in general agreement with the trend observed in $CHFCl_2$ photolysis where it has been found that at the wavelength 213.9 nm the absorption is localized in the C−Cl bond, while at shorter wavelengths C−H bond absorption occurs as well.[5] Similar behavior was found in the photodissociation of CH_3Cl in which at 193 nm no H atoms could be detected[20] while at 157.6 nm appreciable H atom concentrations were observed.[19]

In the 157.6 nm ($\hbar\omega$ = 759.2 kJ/mol) photolysis of all chloromethanes (CH_nCl_{4-n}), "bimodal" H atom Doppler profiles were observed which could be simulated by a superposition of a non-Gaussian and a Gaussian component with the Gaussian component being considerably narrower (fwhm = 4.4−6.4 cm^{-1}) than the non-Gaussian (fwhm = 10.7−13.2 cm^{-1}).[19] The non-Gaussian contribution was attributed to a "direct" photodissociation channel while the Gaussian component was explained by the existence of an "indirect" hot molecule decomposition mechanism suggested by Bersohn and co-workers[21] after excitation to a Rydberg excited state. The bimodal Doppler profiles observed in the present study suggest that at the Lyman-α wavelength the H atom formation in the CHF_2Cl photolysis also proceeds via (at least) two different dissociation mechanisms. In case of CHF_2Cl, Lyman-α radiation leads mainly to A and B band excitation.[7] A-band absorption can be described as valence transitions from a nonbonding chlorine lone pair orbital (n_{Cl}) to a σ^* antibonding orbital with mixed C−H, C−Cl character[11] while B-band absorption at the Lyman-α wavelength can be attributed to a Rydberg process, related to a $n_{Cl} \rightarrow$ 4s transition.[11] The non-Gaussian component could therefore originate from a direct photodissociation process

$$CHF_2Cl + \hbar\omega_{L_\alpha} \rightarrow CHF_2Cl^* \rightarrow CF_2Cl + H \qquad (2)$$

while for the Gaussian component a mechanism such as

$$CHF_2Cl + \hbar\omega_{L_\alpha} \rightarrow CHF_2Cl^{**} \rightarrow CHF_2Cl^{\ddagger} \rightarrow CF_2Cl + H \qquad (3)$$

could be responsible where ** and ‡ indicate electronically excited and "hot" molecular states, respectively, with the electronically excited state ** originating from a $n_{Cl} \rightarrow$ 4s Rydberg excitation. The measured ratio $\Gamma_{non\text{-}G}/\Gamma_G = 1.0 \pm 0.3$ should therefore reflect the ratio of relative absorption of the two electronic transitions involved. In the case of CH_3Cl, for example, lower states of the $n_{Cl} \rightarrow$ 4s Rydberg series have been found to be strongly predissociative.[22] Measurements of H atom Doppler profiles for different pump−probe beam geometries to determine the anisotropy parameters for each H atom channel could provide direct information about the corresponding electronic transitions but are, however, not possible in the present case, as the Lyman-α laser acts as both pump and probe source. Therefore, the following discussion will—because of the lack of information about the actual potential energy surfaces (PESs) involved—be based on the fragmentation energetics and simple statistical models where only energy conservation is incorporated. In Table 1, photochemical H atom reaction channels are listed. The reaction enthalpies were calculated from the standard enthalpies of formation[23] listed in Table 1. Despite being energetically more favorable than C−Cl or C−H bond fission, HCl production was not observed in the 193 nm photolysis of $CHCl_3$, $CHFCl_2$,[9] and CHF_2Cl,[10] and so molecular elimination processes are not taken into account. The ionization potentials for the Cl lone pair and the lowest C−Cl/C−H bonding orbital in CHF_2Cl have been measured to be 12.6 eV (1215.7 kJ/mol) and 14.0 eV (1350.8 kJ/mol), respectively,[11] so ionization of the parent molecule and subsequent ion fragmentation need not be considered in the present study.

TABLE 1: Standard Enthalpies of Formation ΔH°_f and Reaction Enthalpies ΔH_R of Energetically Possible H Atom Product Channels in kJ/mol (Ref 23)

species	ΔH°_f (298 K)	reaction	ΔH_R (298 K)	E_{avl}[a]
CHF_2Cl	−483.7	$CHF_2Cl \rightarrow CF_2Cl + H$	432.7	551.2
CF_2Cl	−269.0	$CHF_2Cl \rightarrow CF_2 + Cl + H$	628.9	355.0
CF_2	−194.1	$CHF_2Cl \rightarrow CFCl + F + H$	803.0	180.9
CFCl	−20	$CF_2Cl \rightarrow CF_2 + Cl$	196.2	
F	79.39	$CF_2Cl \rightarrow CFCl + F$	328.4	
H	217.997			
Cl	121.30			

[a] The available energy to the products is given by $E_{avl} = \hbar\omega_{L_\alpha}$ (983.9 kJ/mol) − ΔH_R (298 K).

The Non-Gaussian Component. Assuming direct H atom formation via reaction 2, the fraction $f_T = E_T/E_{avl}$ of the available energy channeled into H atom translation for the non-Gaussian component is $f_{T(non\text{-}G)} = 0.38$. Comparison of this value with the H atom f_T value of 0.48 obtained at a photolysis wavelength of 193 nm (619 kJ/mol)[11] suggests a similar direct fragmentation dynamics and—because at 193 nm excitation of the $n_{Cl} \rightarrow$ 4s Rydberg transition is energetically not possible[7]—could suggest that also in the VUV wavelength region H atom formation occurs to a certain extent via $n_{Cl} \rightarrow \sigma^*$ excitation. In agreement with the behavior expected for a direct dissociation process on a CHF_2Cl PES that is repulsive along the C−H bond coordinate, the experimental $f_{T(non-G)}$ value is considerably higher than the statistical "prior" value $f_T^{"stat"} = {}^1/_6$ calculated assuming a single C−H bond fission.[24a,25,26] At this point it should be noted that direct H atom production via (2) following Lyman-α excitation actually leaves the CF_2Cl radical with a total internal energy E_{int} of up to 344.2 kJ/mol. $E_{int} = E_{avl} - E_{t(c.m.)}$ was calculated using the reaction enthalpy given in Table 1, and $E_{t(c.m.)} \approx E_{T(non-G)}$ = 207 kJ/mol for the center-of-mass translational energy, the approximation being justified because of the large mass ratio m_{CF_2Cl}/m_H.E_{int} is high enough (see Table 1) to allow Cl and F atom formation by subsequent decomposition of the CF_2Cl fragment. Thus, the complete photochemical reaction could be described by the following "sequential" decay mechanism:

$$CHF_2Cl + \hbar\omega_{L_\alpha} \rightarrow CHF_2Cl^* \rightarrow CF_2Cl^{\ddagger} + H \qquad (4a)$$

$$CF_2Cl^{\ddagger} \rightarrow CF_2 + Cl \qquad (4b)$$

$$CF_2Cl^{\ddagger} \rightarrow CFCl + F \qquad (4c)$$

Here sequential[27] means that the overall process proceeds by a sequence of two independent steps (4a followed by b or c) where the decay of $CF_2Cl^{\ddagger}$ is not influenced by the first fragment (the H atom in our case). In this case, reaction step 4a can be considered to be a "fast" single C−H bond fission process, followed by the second step (4b or 4c) which then can be considered as a subsequent unimolecular reaction where the rates $k(E_{int})$ may be calculated using statistical theories (e.g., RRKM,[28] PST,[29] SACM[30]) if the excited molecules live long enough to allow for a complete randomization of the internal energy before the decomposition.

The Gaussian Component: A Predissociation Mechanism for CHF_2Cl Photodissociation. The solid curve in Figure 4c represents the Maxwell−Boltzmann-like H atom velocity distribution derived from the Gaussian component of the Doppler profile fit (Figure 4a). This distribution is characteristic of a translational "temperature" of about 5900 K, corresponding to an average energy of $E_{T(G)} = {}^3/_2RT = 74$ kJ/mol. The dashed lines i and ii in Figure 4c are statistical "prior" distributions $P(E_T|E_{avl})$ calculated for the following two energetically possible H atom producing "simultaneous" three-body processes taking into account rigorous conservation of E_{avl} only:[25]

$$CHF_2Cl^{\ddagger} \rightarrow CF_2 + Cl + H \quad (5)$$

$$CHF_2Cl^{\ddagger} \rightarrow CClF + F + H \quad (6)$$

Using the "canonical" statistical model of Baer et al.[24b] in which the constraint of rigorous conservation of E_{avl} is replaced by conservation of the average internal energy gave a translational temperature of about 5700 K for reaction 5 and 2900 K for reaction 6 assuming simultaneous three-body dissociation. In order to allow the application of statistical methods, it has to be assumed, of course, that the excited molecule ($CHF_2Cl^{\ddagger}$) lives long enough to allow for a complete randomization of the internal energy before it breaks apart. The good agreement with the statistical predictions might suggest that the Gaussian component of the measured H atom profiles originates mainly from statistical three-body decay (5)—maybe with some contribution from (6)—after Rydberg excitation.

Conclusion

Using the laser photolysis/laser-induced fluorescence "pump/probe" technique, we measured a total H atom quantum yield of $\Phi_H = 0.77 \pm 0.13$ for the dissociation of CHF_2Cl following photoexcitation at the Lyman-α wavelength. The relatively high value of Φ_H suggests CHF_2Cl to be an efficient precursor of translationally excited H(^{2}S) atoms in the earth's stratosphere.

Under collision-free conditions, bimodal H atom Doppler profiles were observed. An analysis of the bimodal H atom Doppler profiles suggests that H atom formation proceeds via two distinct photochemical channels, of approximately equal probability. It is suggested that the two H atom channels originate from the excitation of two different electronic transitions, namely, a transition that excites to a state which is repulsive in the C−H coordinate in the case of the nonstatistical "fast" H atom Doppler profile component and a transition that excites to a state leading to H atom formation via a predissociation mechanism in the case of the statistical "slow" H atom velocity contribution. However, for a definite assignment of the two optical VUV transitions involved, theoretical and further experimental studies for different pump−probe beam geometries, using for example a polarized 157.6 nm F_2 excimer laser as an independent photolysis light source, in order to determine the corresponding H atom fragment anisotropy parameters would be desirable.

Acknowledgment. We thank P. Farmanara for help in the experiments, A. Melchior for helpful communications, and Professor Y. T. Lee and Professor Y. Matsumi for sending preprints of their work. R.K.V. acknowledges a fellowship provided by the KFA Jülich and DLR Bonn under the Indo-German bilateral agreement (Project CHEM-19). The authors gratefully acknowledge financial support of the European Union under Contract ISC*-CT940096 of the International Scientific Cooperation programme.

References and Notes

(1) Wayne, R. P. *The Chemistry of Atmospheres*, 2nd ed.; Oxford University Press: Oxford, 1991 and references therein.
(2) Manzer, L. *Science* **1990**, *249*, 31.
(3) *ATLAS 3 Public affairs status report* #20, NASA Science Operations Marshall Space Flight Center, Huntsville, Nov 13, 1994.
(4) *Energie und Klima: Erster Zwischenbericht der Bundestag-Enquet-Kommission "Vorsorge zum Schutz der Erdatmosphäre"*; Economica Verlag: Bonn, 1990.
(5) (a) Okabe, H. *Photochemistry of Small Molecules*; John Wiley & Sons: New York, 1978. (b) *Scientific Assessment of Ozon Depletion: 1991*, World *Meteorological* Organization Global Research and Monitoring Project Report No. 25, World Meteorological Organization, Geneva, Switzerland, 1992.
(6) Robbins, D. E.; Stolarski, R. S. *Geophys. Res. Lett.* **1976**, *3*, 603. Hubrich, C.; Zetzsch, C.; Stuhl, F. *Ber. Bunsen.-Ges. Phys. Chem.* **1977**, *81*, 437. Greene, R. G.; Wayne, R. P. *J. Photochem.* **1977**, *6*, 375.
(7) Robin, M. B. *Higher Excited States of Polyatomic Molecules*; Academic Press: New York, 1974; Vol. I.
(8) DeMore, W. B.; Sander, S. P.; Golden, D. M.; Hampson, R. F.; Kurylo, M. J.; Howard, C. J.; Ravishankara, A. R.; Kolb, C. E.; Molina, M. J. *Chemical Kinetics and Photochemical Data for Use in Stratospheric Modeling, No. 10*, NASA, JPL Publication 92−20, 1992.
(9) Yang, X.; Felder, P.; Huber, J. R. *Chem. Phys.* **1994**, *189*, 129.
(10) Melchior, A.; Knupfer, P.; Bar, I.; Rosenwaks, S.; Laurent, T.; Volpp, H.-R.; Wolfrum, J. *J. Phys. Chem.* **1996**, *100*, 13375.
(11) Doucet, J.; Sauvageau, P.; Sandorfy, C. *J. Chem. Phys.* **1973**, *58*, 3708.
(12) Gilbert, R.; Sauvageau, P.; Sandorfy, C. *J. Chem. Phys.* **1974**, *60*, 4820.
(13) (a) Laurent, T.; Naik, P. D.; Volpp, H.-R.; Wolfrum, J.; Arusi-Parpar, T.; Bar, I.; Rosenwaks, S. *Chem. Phys. Lett.* **1995**, *236*, 343. (b) Brownsword, R. A.; Laurent, T.; Vatsa, R. K.; Volpp, H.-R.; Wolfrum, J. *Chem. Phys. Lett.* **1996**, *258*, 164.
(14) Volpp, H.-R.; Wolfrum, J. In *Gas Phase Chemical Reaction Systems: Experiments and Models 100 Years after Max Bodenstein*; Wolfrum, J., Volpp, H.-R., Rannacher, R., Warnatz, J., Eds.; *Springer Ser. Chem. Phys.* **1996**, *61*.
(15) Hilber, G.; Lago, A.; Wallenstein, R. *J. Opt. Soc. Am. B* **1987**, *4*, 1753. Marangos, J. P.; Shen, N.; Ma, H.; Hutchison, M. H. R.; Connerade, J. P. *J. Opt. Soc. Am. B* **1990**, *7*, 1254.
(16) (a) Andresen, P.; Ondrey, G. S.; Titze, B.; Rothe, E. W. *J. Chem. Phys.* **1984**, *80*, 2548. (b) Docker, M. P.; Hodgson, A.; Simons, J. P. In *Molecular Photodissociation Dynamics*; Ashfold, M. N. R., Baggot, J. E., Eds.; Royal Society of Chemistry: London, 1987. (c) Engel, V.; Staemmler, V.; Van der Wal, R. L.; Crim, F. F.; Sension, R. J.; Hudson, B.; Andresen, P.; Henning, S.; Weide, K.; Schinke, R. *J. Phys. Chem.* **1992**, *96*, 3201. (d) Schinke, R. *Photodissociation Dynamics Spectroscopy and Fragmentation of Small Polyatomic Molecules*; Cambridge University Press: Cambridge, 1993 and references therein.
(17) Mordaunt, D. H.; Ashfold, M. N. R.; Dixon, R. N. *J. Chem. Phys.* **1994**, *100*, 7360.
(18) Slanger, T. G.; Black, G. *J. Chem. Phys.* **1982**, *77*, 2432.
(19) Tonokura, K.; Mo, Y.; Matsumi, Y.; Kawasaki, M. *J. Phys. Chem.* **1992**, *96*, 6688.
(20) Continetti, R. E.; Balko, B.; Lee, Y. T. *J. Chem. Phys.* **1988**, *89*, 3383.
(21) Yi, W.; Chattophadhay, A.; Bersohn, R. *J. Chem. Phys.* **1991**, *94*, 5994.
(22) Herzberg, G. *Molecular Spectra and Molecular Structure*; Van Nostrand: Toronto, 1966; Vol. III.
(23) Atkinson, R.; Baulch, D. L.; Cox, R. A.; Hampson, R. F., Jr.; Kerr, J. A.; Troe, J. *J. Phys. Chem. Ref. Data* **1992**, *21*, 1125.
(24) (a) Silberstein, J.; Levine, R. D. *Chem. Phys. Lett.* **1980**, *74*, 6. (b) Baer, T.; Depristo, A. E.; Hermans, J. J. *J. Chem. Phys.* **1982**, *76*, 5917.
(25) Levine, R. D.; Kinsey, J. L. In *Atom-Molecule Collision Theory—A Guide for the Experimentalist*; Bernstein, R. B., Ed.; Plenum Press: New York, 1979. Levine, R. D.; Bernstein, R. B. *Molecular Reaction Dynamics and Chemical Reactivity*; Oxford University Press: Oxford, 1987.
(26) Muckermann, J. T. *J. Phys. Chem.* **1989**, *93*, 180.
(27) Dewar, M. J. S. *J. Am. Chem. Soc.* **1984**, *106*, 205.
(28) Gilbert, R. G.; Smith, S. C. *Theory of Unimolecular and Recombination Reactions*; Blackwell Scientific: Oxford, 1990 and references therein.
(29) Nikitin, E. E. *Teor. Eksp. Khim.* **1965**, *1*, 134. Pechukas, P.; Light, J. C. *J. Chem. Phys.* **1965**, *42*, 3281.
(30) Quack, M.; Troe, J. *Ber. Bunsen-Ges. Phys. Chem.* **1975**, *70*, 912. Troe, J. *J. Chem. Phys.* **1983**, *79*, 6017.